Title

3D-printed breast phantom for multi-purpose and multi-modality imaging

Authors

He, Yaoyao
Liu, Yulin
Dyer, Brandon A
et al.

3D-printed breast phantom for multi-purpose and multi-modality imaging

Yaoyao He[1#], Yulin Liu[2#], Brandon A. Dyer[3], John M. Boone[4], Shanshan Liu[5], Tiao Chen[1,2], Fenglian Zheng[1], Ye Zhu[1], Yong Sun[1], Yi Rong[3], Jianfeng Qiu[1]

[1]Medical Engineering and Technology Center, Taishan Medical University, Taian 271016, China; [2]Department of Radiology, Hubei Cancer Hospital, Wuhan 430079, China; [3]Department of Radiation Oncology, University of California Davis Medical Center, Sacramento, CA 95630, USA; [4]Department of Radiology, University of California Davis Medical Center, Sacramento, California 95817, USA; [5]Department of Radiology, Affiliated Hospital of Taishan Medical University, Taian 271016, China

[#]These authors contributed equally to this work.

Correspondence to: Jianfeng Qiu, PhD. Taishan Medical University, No. 619, Changcheng Road, Taian 271016, China. Email: jfqiu100@gmail.com; Yi Rong, PhD. University of California Davis Medical Center, 4501 X Street, Sacramento, CA 95817, USA. Email: yrong@ucdavis.edu.

Background: Breast imaging technology plays an important role in breast cancer planning and treatment. Recently, three-dimensional (3D) printing technology has become a trending issue in phantom constructions for medical applications, with its advantages of being customizable and cost-efficient. However, there is no current practice in the field of multi-purpose breast phantom for quality control (QC) in multi-modalities imaging. The purpose of this study was to fabricate a multi-purpose breast phantom with tissue-equivalent materials via a 3D printing technique for QC in multi-modalities imaging.

Methods: We used polyvinyl chloride (PVC) based materials and a 3D printing technique to construct a breast phantom. The phantom incorporates structures imaged in the female breast such as microcalcifications, fiber lesions, and tumors with different sizes. Moreover, the phantom was used to assess the sensitivity of lesion detection, depth resolution, and detectability thresholds with different imaging modalities. Phantom tissue equivalent properties were determined using computed tomography (CT) attenuation [Hounsfield unit (HU)] and magnetic resonance imaging (MRI) relaxation times.

Results: The 3D-printed breast phantom had an average background value of 36.2 HU, which is close to that of glandular breast tissue (40 HU). T1 and T2 relaxation times had an average relaxation time of 206.81±17.50 and 20.22±5.74 ms, respectively. Mammographic imaging had improved detection of microcalcification compared with ultrasound and MRI with multiple sequences [T1WI, T2WI and short inversion time inversion recovery (STIR)]. Soft-tissue lesion detection and cylindrical tumor contrast were superior with mammography and MRI compared to ultrasound. Hemispherical tumor detection was similar regardless of the imaging modality used.

Conclusions: We developed a multi-purpose breast phantom using a 3D printing technique and determined its value for multi-modal breast imaging studies.

Keywords: Breast phantom; 3D printing; magnetic resonance imaging (MRI); mammography; polyvinyl chloride (PVC); ultrasound

Introduction

Breast cancer is one of the most common cancers in women worldwide, accounting for 25% of diagnosed cancer cases and 15% of cancer-related deaths among women (1). Although routine mammography, which remains the primary diagnostic and screening tool for breast cancer (1), has the ability to detect early stage breast cancer (2) and reduce the incidence of late-stage breast cancer (3), it has limited sensitivity in detecting lesions in women with dense breasts (4). Ultrasound and magnetic resonance imaging (MRI) can be used as alternative modalities for mammography in these patients (1,5,6). Breast ultrasound imaging can assist in distinguishing between cysts and solid masses, potentially reducing unnecessary biopsies (7,8). With the ability to detect breast cancers at the pre-invasive stage, MRI has been used as an adjunct to mammographic screening, especially in women with a high risk of breast cancer (9,10). Furthermore, dynamic contrast-enhanced MRI (DCE-MRI) images provide vascular kinetics in tissues, which improves tumor detection capability and sensitivity (9,11). Routine incorporation of MRI should be approached cautiously as it can increase diagnostic costs, biopsies and mastectomy rates without changing the survival or recurrence endpoints (12). However, Kolb *et al.* (4) and Berg *et al.* (13) compared combined breast evaluation applications including clinical examination, ultrasound, MRI, and multi-modal combination with the use of a single modality and their results indicated improved sensitivity in cancer detection with the combination of modalities.

These studies emphasize the urgent need for a quantitative and qualitative phantom for imaging quality assessment and testing (14,15). Currently, the majority of phantoms are designed for use with a single imaging modality; thus, multiple purpose phantoms are required for different imaging systems. Several commercialized breast phantoms have been developed using tissue-mimicking materials (TMMs) for adipose and glandular tissue for use with specific imaging techniques. With mammography, polymethyl methacrylate (PMMA) plates (16-18) and epoxy resins (19-21) are the TMMs commonly used to represent different proportions of adipose and glandular tissue. In breast ultrasound, TMMs include biopolymers [gelatin (22) and agar (23,24)], polyacrylamides (25), urethane rubber (26), and paraffin–gel waxes (27). Similar MRI phantoms have been designed with homogeneous glandular-equivalent tissues (i.e., polysaccharides, water, and egg whites) which are surrounded by homogeneous adipose-equivalent tissue (i.e., Crisco, fat, and lard) (28-32). However, all these phantoms are only compatible with a single-modality imaging system. Furthermore, some of the TMMs in use, such as PMMA, are poor surrogates for breast tissue (33).

To overcome these limitations, construction of multi-modal breast phantoms has been pursued (19,34-36). Biopolymers are commonly used to construct these multi-modal breast phantoms with TMMs (22-24,30,35,36), but have poor durability due to water evaporation and bacterial growth (36-38). Unlike these biopolymers, polyvinyl chloride (PVC), a common synthetic chemical polymer, is easy to handle, bacterial-resistant, stable and durable under normal, ambient conditions (39).

Here, we use PVC-based TMM material and three-dimensional (3D) printing techniques to construct a custom-designed breast phantom with multiple inserts for multi-modal image quality control (QC) (i.e., mammography, MRI, ultrasound). To our knowledge, there has been no publication in the literature addressing the need for constructing a breast phantom for multi-modality imaging QC with cost-efficiency and ease of customization.

Methods

Phantom construction

Production of PVC-based materials as TMM

The soft PVC TMM used for phantom construction was made from a mixture of PVC powder and softener (i.e., dioctyl terephthalate). A mixture of white and opaque PVC powder and softener was heated to 280 ℃ on a laboratory hot plate with constant stirring until the mixture was thoroughly polymerized and transparent (40). For breast ultrasound imaging, 3% graphite powder was added to the mixture resulting in an echo speed of 1,397.9 m/s (41), which provides sharp contrast with the insert and mimics breast tissue. A 3D-printed negative breast mold (described in section 2.1.2 and 2.1.4) was coated with Vaseline, then preheated before being filled in with the PVC mixture. This was allowed to cool at room temperature, forming the breast phantom.

Breast mold design

An anonymized MRI scan of a female breast was obtained from the Cancer Imaging Archive (TCIA) (42,43). The TCIA is a public database that does not require ethics approval. The MRI dataset was imported into Materialise Mimics (17.0.0.435, Materialise, Leuven, Belgium) for structure segmentation, smoothing, and remeshing for 3D
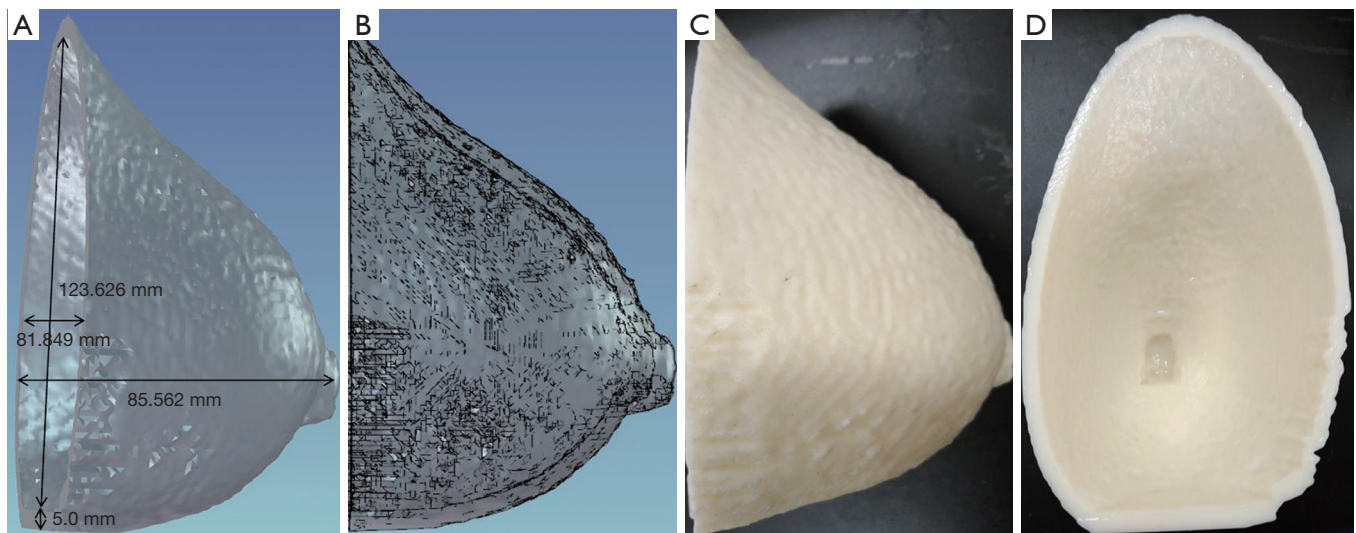
Figure 1 The breast mold. (A,B) 3D rendering of the breast mold; (C,D) photographs of the 3D-printed breast mold.

printing of the breast mold (*Figure 1*).

Insert generation

Embedded inserts (semi-elliptic cylinder, height 53 mm, width 50 mm, thickness 6.0 mm) were generated to simulate tumors. A total of 18 cylindrical (columns 1–3) and 18 hemispherical (columns 4–6) holes were imbedded in the insert ranging in diameter from 2.0 to 6.0 mm. For depth resolution, a total of 72 cylinders with 8 cylinders per row and a thickness ranging from 0.25 to 5.0 mm were used. Columns of 9 cylinders with diameters ranging from 1.0 to 5.0 mm were used. For fiber lesions, a total of 15 horizontal strips ranging in height from 0.2 to 1.6 mm were used. For microcalcifications, a total of 17 groups of calcifications, each group containing 8 cylinders ranging in diameter from 1.2 to 2.1 mm were used. The 3D-printed inserts were designed using SolidWorks software (SolidWorks, SolidWorks Corp., Concord, MA, USA). Inserts were used to evaluate imaging quality and detection sensitivity based on lesion size, depth resolution, and threshold detection ability in different imaging systems (*Figure 2*).

3D printing

The 3D breast mold segmentation and inserts' mesh files were converted to Standard Tessellation Language (STL) format compatible with the 3D printer (Objet 50, Stratasys, Minneapolis, Minnesota, USA). Acrylonitrile butadiene styrene (ABS) was used to print the 3D breast mold and inserts using 100% infill density with a fused deposition

printing technique. The printing accuracy was 0.256 mm.

Image acquisition and evaluation

Mammography

A MAMMOMAT Inspiration system (Siemens AG, Erlangen, Germany) was used to acquire mediolateral oblique (MLO) and cranio-caudal (CC) images as shown in *Figure 3*. The mammographic scanning parameters included 28.0 kV, 168.0 mAs, 77.4–90.1 N for the compression force.

MRI

MRI images of the breast phantom were acquired using a 3.0 T Siemens Magnetom Verio scanner (Siemens, Erlangen, Germany) with a proprietary phase array breast coil. T1WI, T2WI and short inversion time inversion recovery (STIR) sequences were obtained. Additionally, T1 and T2 time constant measurements were obtained using a 16-channel head coil. MRI parameters are listed in *Table 1*.

Ultrasound

A high-resolution ultrasonic diagnostic instrument (Mindray DC-N3 Doppler) was used with the transducer operating at a central frequency of 7.5 MHz.

Image evaluation and statistical analysis

In this study, mammography images were assessed by a mammography specialist, ultrasound images were gauged by a sonographer, and MRI images were evaluated by a
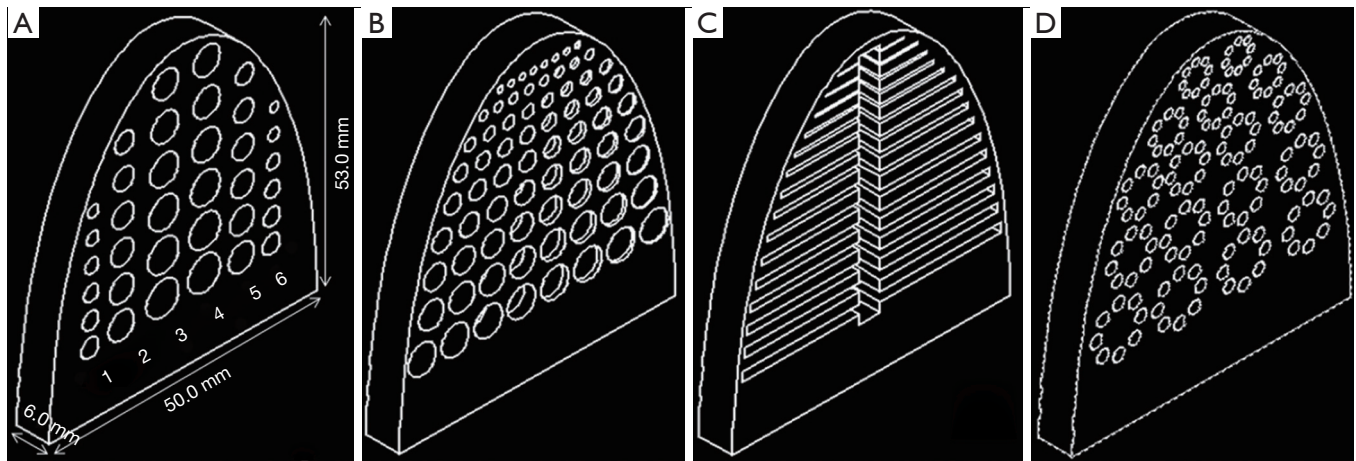
Figure 2 3D illustration of the breast phantom inserts. (A) Simulated tumors: cylindrical holes (column 1–3), and hemispherical holes (column 4–6). Diameters range from 2.0–6.0 mm. (B) Depth resolution: eight cylinders per row with thickness ranging from 0.25–5.0 mm. Each column contains nine cylinders with diameters ranging from 1.0–5.0 mm. (C) Fibers: strips with widths ranging from 0.2–1.6 mm. (D) Microcalcifications: each group contains eight cylinders with diameters ranging from 1.6–2.1 mm and 5.0 mm thickness.
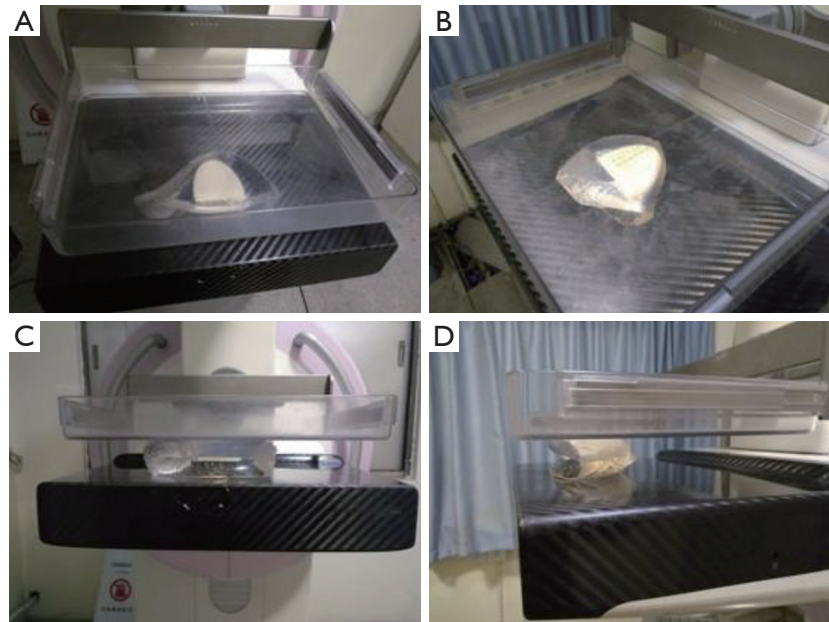
Figure 3 Breast phantom mammography using 28.0 kV, 168.0 mAs in (A) MLO and (B) CC positions. (C,D) The breast phantom is capable of compression for mammography.

radiologist. Each specialist has more than 5 years of clinical experience and expertise in their corresponding imaging modality.

All data were collected and analyzed using GraphPad Prism 7 (Graphpad Prism, Graphpad Prism Software Inc., San Diego, CA, USA).

Results

PVC-softener ratio selection

The PVC-softener ratio greatly affects imaging physics properties of studied materials (39). The ratio most closely resembling biologic breast and tumor characteristics

Table 1 MRI acquisition parameters

Parameter	Image acquisition[†]			Relaxation time[†]	
	T1-weighted	T2-weighted	STIR	T1-mapping	T2-mapping
TR (ms)	6.1	4,500	8.75	15	1,000
TE (ms)	2.6	70	4.33	2.32	13.8, 27.6, 41.4, 55.2, 69.0
Slice thickness (mm)	4	4	0.9	3	3
Flip angle (°)	15	120	15	5	180
NEX	1	1	1	1	1

[†], Siemens Magnetom Verio. NEX, number of excitation.

Table 2 Breast phantom characteristics

Breast phantom/ characteristic of TMMs	PVC-softener ratio (×10⁻² g/mL)	Imaging characteristic	Measured value	Published value
Background	12.3	CT number (HU)	+36.2	+40 (36)
		T1 (ms)	206.81±17.50	1,324.42±167.63 (44)
		T2 (ms)	20.22±5.74	54.36±9.35 (44)
	12.3 (3.0% graphite power)	Speed of sound (m/s)	1,397.9 (41)	1,544 (45,46)
Tumor	15.2	CT number (HU)	+59.4	+10 to +60 (36,47)

were chosen, as shown in *Table 2*. A PVC-softener ratio of 12.3×10^{-2} g/mL (i.e., 49.2 g PVC in 400 mL softener) corresponds to 36.2 HU and closely resembles glandular tissues (40 HU) (36). Depending on the tissue of interest, breast models using various materials (e.g., PVC and agar) can be combined to accurately create an imaging phantom with similar imaging characteristics (CT number, T1-/T2- relaxation, m/s, etc.). In this experiment, a PVC-softener ratio of 15.2×10^{-2} g/mL (59.4 HU) was chosen, which is also close to the attenuation of actual tumor (60 HU) (36,47).

Phantom construction

The breast phantom was made of TMMs with PVC-based materials to mimic glandular breast tissue. Various QC inserts were incorporated to mimic artificial features (e.g., microcalcifications, fiber lesions, or tumors), and provided qualitative assessment of the lesion detection sensitivity for various imaging modalities (i.e., depth resolution). An interlock system was used to ensure insert alignment. *Figure 4* shows a multi-purpose bulk breast phantom with various QC inserts.

Simulated lesions

Four types of inserts were used to evaluate imaging,

in detail, of characteristics of simulated tumors, depth resolution, fiber lesions and microcalcifications, for mammography (*Figure 5*), MRI (*Figure 6*), and ultrasound (*Figure 7*). All the results of the detected simulated lesions are summarized in *Figure 8*, which shows the comparison of three imaging modalities in image QC performance with various inserts.

Mammography

One hundred percent of cylindrical tumors, 88.9% of hemispherical tumors (*Figure 5A,E*), 100% of fiber lesions (*Figure 5C,G*), and 100% of microcalcifications (*Figure 5D,H*) were detected. Of the cases with depths from 0.5 to 5.0 mm and sizes from 0.25 to 5.0 mm, 65.3% were detected in depth resolution insert (*Figures 5B,F*).

MRI

One hundred percent of cylindrical tumors and 83.3% of hemispherical tumors were detected with MRI images (*Figure 6A,E,I*). For depth resolution, 94.4%, 66.7%, and 88.9% of cases were detected on T1-weighted (*Figure 6B*), T2-weighted (*Figure 6F*), and STIR (*Figure 6J*) images, respectively. Of the simulated fiber lesions, 100%, 93.3%, and 93.3% were detected with T1-weighted (*Figure 6C*), T2-weighted (*Figure 6G*) and STIR (*Figure 6K*) images,
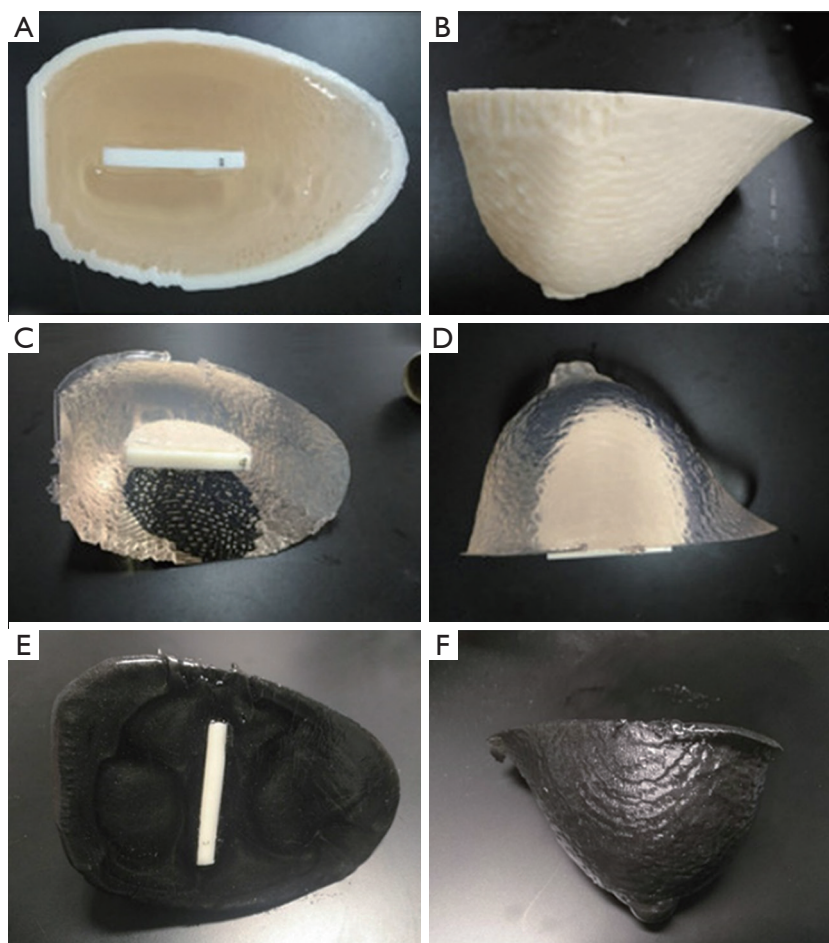
Figure 4 Photographs of the breast phantom. (A,B) The breast phantom and insert within the breast mold. (C,D) The PVC breast phantom has been removed from the mold and is ready for mammography and MRI. (E,F) An ultrasound breast phantom uses the mixture of PVC, softener and 3.0% graphite power to improve tissue contrast for imaging.

respectively. For microcalcifications, 76.5% were detected both on T1-weighted and STIR images (*Figure 6D,L*); however, only 13.2% of cases were detected with T2-weighted images (*Figure 6H*).

Ultrasound

Using ultrasound, 94.4% of simulated cylindrical tumors, 83.3% of hemispherical tumors (*Figure 7A*), 66.7% in depth resolution (*Figure 7B*), and 45.6% of microcalcifications (*Figure 7D*) were detected. For fiber lesions, cases with diameters ranging from 0.8 to 1.5 mm had 60% detection (*Figure 7C*).

Discussion

In this study, we designed and constructed a novel multi-

modal compatible tissue-equivalent breast phantom with embedded inserts for simulating different breast lesions. We further analyzed quantitative and qualitative imaging characteristics for biophysically-equivalent simulated breast lesions using this multi-modal breast imaging phantom with various acquisition techniques. Our results showed that mammographic images showed a higher number of visible microcalcifications than those in the ultrasound and MRI. Visualization of lesions was improved with mammography and MRI versus ultrasound. The contrast of simulated cylindrical tumors with mammography and MRI was superior compared to ultrasound, and visualization of hemispherical tumors was similar in the various systems. A combination of different imaging modalities is recommended to improve the sensitivity of lesion detection.

3D printing techniques play an increasingly important
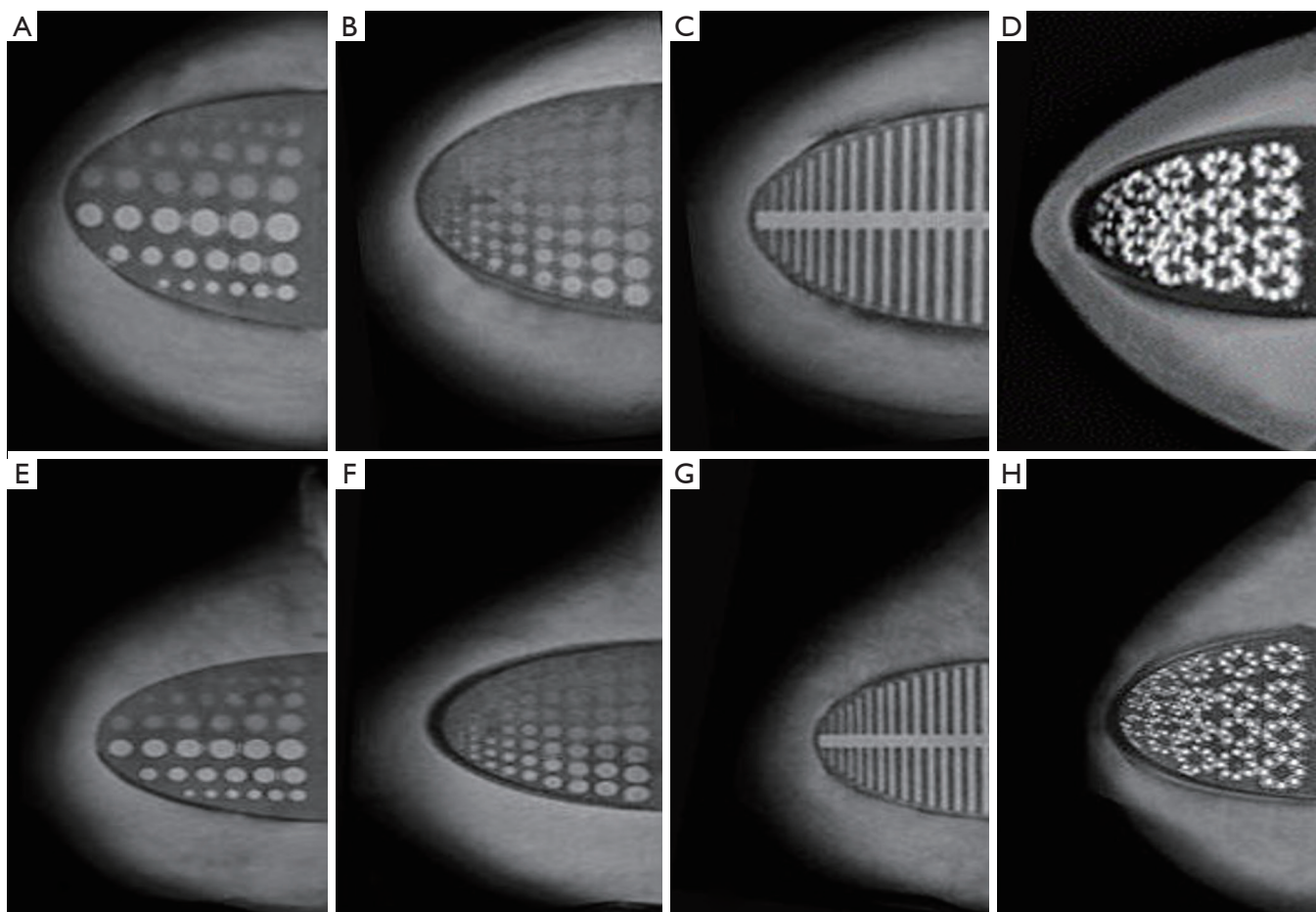
Figure 5 (A,B,C,D) CC and (E,F,G,H) MLO mammographic images of the multi-modal breast phantom (28 kV, 168 mA). Tumor inserts (A) and (E), depth resolution inserts (B) and (F), fiber inserts (C) and (G), and microcalcification inserts (D) and (H) are used for qualitative measurements.

role in phantom constructions for clinical applications. Medical application of 3D printing technology is feasible for proton range compensators (44), pre-surgical planning (45,46), prosthetics/dental implants (48,49), and medical phantoms (50). With the advantages of being customizable and cost-efficient, 3D-printed phantom has significant contribute to equipment correction, patient-clinician interaction, tissue substitute, medical research and medical education/training (51). This technique was used in this study to construct the breast phantom mold, in addition to phantom inserts. The phantom was tested using different imaging modalities for breast imaging, and this represents the novel aspect of our study.

Another important part of this study was to develop TMMs for human breast. PVC is one of the most common and widely used materials in phantoms, including

abdominal phantoms for registration accuracy (52), prostate phantoms for image-guided biopsy procedures (53), and the mixture of PVC plastisol and graphite powder for ultrasound imaging (41). However, to our knowledge, there have been no published studies reporting appropriate TMMs for breast phantoms. In our study, we identified and reported a PVC-softener mixture that represents the physical and imaging properties of human breast tissues. A PVC-softener ratio of 12.3×10^{-2} g/mL corresponds to 36.2 HU, which is similar to previous results from Liao *et al.* (40), and also close to glandular tissues (40 HU) (36). Although the T1 and T2 relaxation times are shorter than those reported with physiologic breast tissue (54), we found the mean relaxation times of 206.81±17.50 ms for T1 and 20.22±5.74 ms for T2, as compared to published values of 1,324.42±167.63 ms and 54.36±9.35 ms, respectively (54).
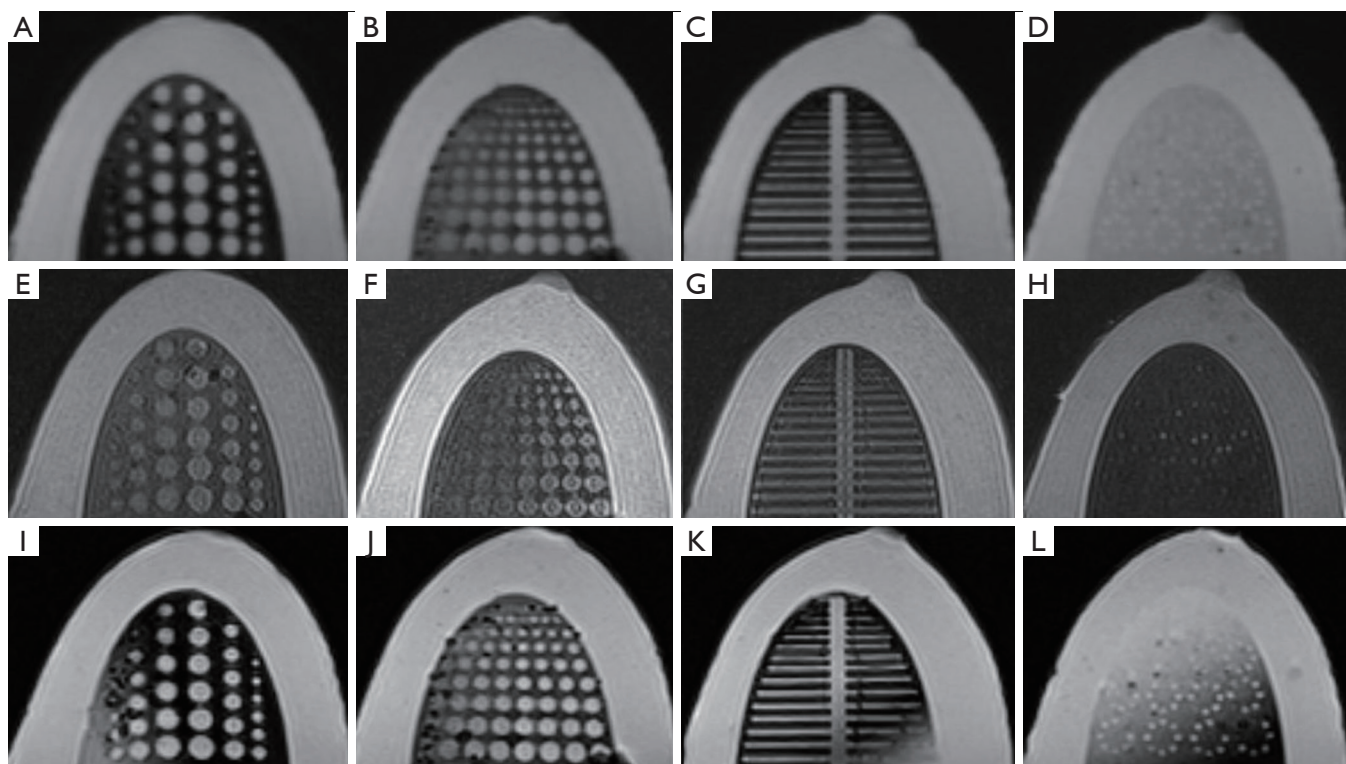
Figure 6 MRI images of the multi-modal breast phantom with T1WI (A,B,C,D), T2WI (E,F,G,H), and STIR (I,J,K,L) sequences. The first column (A,E,I) shows tumor inserts, the second column (B,F,J) shows depth resolution inserts, the third column (C,G,K) shows fiber inserts, and the forth column (D,H,L) shows microcalcification inserts.
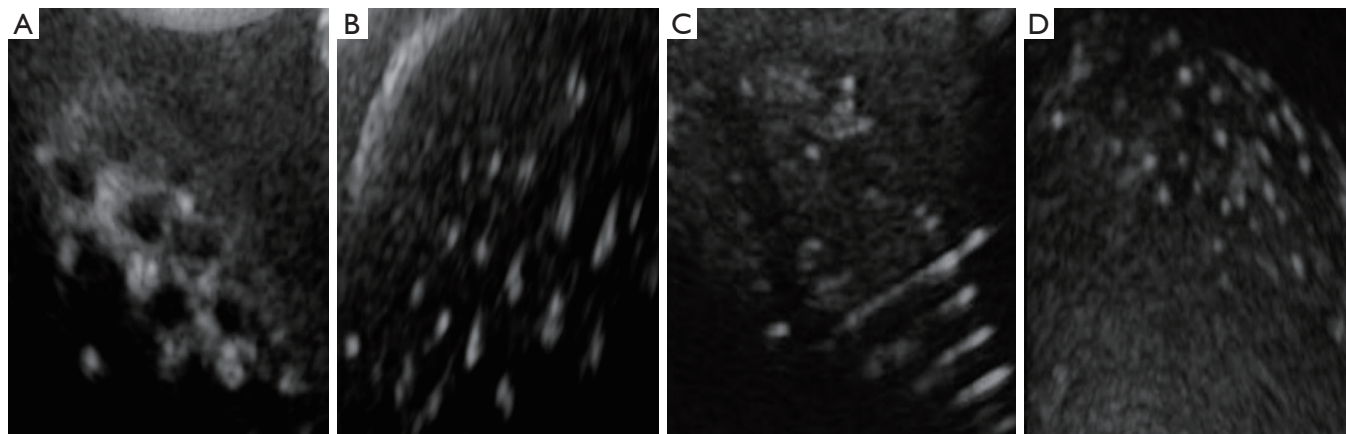
Figure 7 Ultrasound images of the multi-modal breast phantom. (A) Tumor inserts, (B) depth resolution inserts, (C) fiber inserts, (D) microcalcification inserts.

The speed of sound in PVC measured by anechoic imaging is approximately 1,400 m/s (39,53,55,56), which is lower than that of human glandular tissue at 1,544 m/s (57,58). For ultrasound imaging, a 3.0% graphite power was added to the PVC-softener ratio resulting in an echo speed of 1,397.9 m/s with hyperechoic imaging (41). This step, while providing a sharp contrast with the inserts, may not truly reflect the biophysical imaging characteristics of
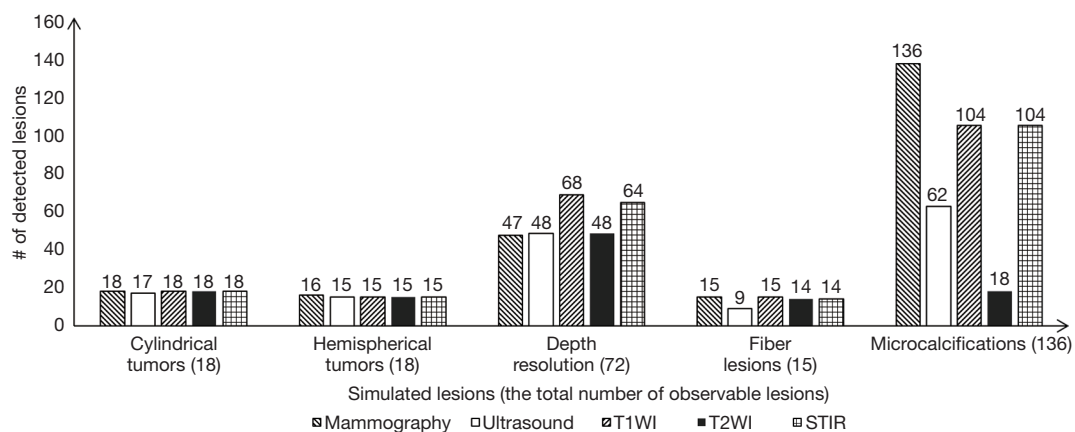
Figure 8 Comparison of the number of detected simulated lesions in different modalities.

human tissue. Therefore, an opportunity for further TMM development and more sophisticated 3D printed breast phantom development exists.

The benefit of using PVC-based material for mammography is that due to its inherent elasticity, the breast phantom can be compressed for mammographic imaging. Freed *et al.* (34) described a dual-modality breast phantom capable of compression; however, the resulting deformation after compression was not compatible with mammographic imaging. Our PVC-based breast phantom is superior to those previously described (28,34,36) although the overall elastic deformation capability is relatively limited and still needs future development. If the pressure applied to the phantom for mammographic imaging exceeds the elastic modulus of this material, the phantom may be damaged.

Typical evaluation criteria for a breast phantom include QC (16,28), detectability of microcalcifications, masses (16,17,59-63), and assessment/optimization of MRI acquisition protocols (29,30). Our breast phantom was designed to evaluate imaging characteristics of a single breast lesion for mammography, MRI, and ultrasound, including simulated tumors, depth resolution, fiber lesions, and microcalcifications. For simulated tumors, more than 94% of cylindrical cases and more than 83% of hemispherical cases were detected for all three imaging modalities. For depth resolution, depths greater than 0.5 mm and diameters greater than 1.5 mm were detected for all three imaging modalities. MRI had the best performance due to 3D image acquisition, but detection performance varied with the MRI acquisition sequence. For fiber lesions, diameters greater than 0.8 mm were detected for all three

imaging modalities. The imaging performance in detecting microcalcifications was variable depending on the imaging modality used. In general, lesion diameters greater than 1.6 mm were detected with all modalities, and mammography outperformed ultrasound and MRI. Finally, ultrasound had good detection performance for fiber lesions, depth resolution, and tumors; however, feature details lacked imaging contrast and this method was not sensitive to small lesions.

Despite robust qualitative measurements there are some limitations to the current study. 3D printing has an accuracy of 0.256 mm and limits the ability to assess micrometer lesions. In addition, the current phantom was constructed with a homogenous density and lacks the heterogeneity present in physiologic tissues. Incorporation of heterogeneous materials through advanced 3D printing techniques will improve phantom design and biophysical equivalence compared with physiologic tissues. Finally, a temperature difference between the PVC-softener mixture and breast mold may introduce bubbles which cannot be eliminated, and this may affect image quality. It is worth noting that the presence of bubbles can be minimized by reducing excessive mixing during heating, preheating the breast mold, or placing the PVC mixture under a strong vacuum prior to decanting into breast mold.

Conclusions

We constructed an anthropomorphic PVC breast phantom using 3D printing and TMMs capable of multi-modal imaging assessment for mammography, MRI, and ultrasound. Embedded inserts allow for qualitative image

assessments. Ongoing development of a heterogeneous breast phantom using high-fidelity 3D printing with multiple biologically-equivalent materials will improve the phantom similarity to physiologic tissues, and thus further enhance image quality and lesion detection.

Acknowledgements

We would like to thank Haozhao Zhang, Fuquan Zhang, Xiaojing Liu, and Liting Shi for their comments and suggestions.

Footnote

Conflicts of Interest: The authors have no conflicts of interest to declare.

Ethical Statement: The TCIA is a public database that does not require ethics approval.

References

1. Stewart B, Wild CP. editor. World Cancer Report 2014. International Agency for Research on Cancer, WHO 2014:Chapter 5.12: 470-6.
2. Day N, Warren R. Mammographic screening and mammographic patterns. Breast Cancer Res 2000;2:247-51.
3. Bleyer A, Welch HG. Effect of three decades of screening mammography on breast-cancer incidence. N Engl J Med 2012;367:1998-2005.
4. Kolb TM, Lichy J, Newhouse J. Comparison of the performance of screening mammography, physical examination, and breast US and evaluation of factors that influence them: an analysis of 27,825 patient evaluations. Radiology 2002;225:165-75.
5. Warner E, Plewes DB, Hill KA, Causer PA, Zubovits JT, Jong RA, Cutrara MR, DeBoer G, Yaffe MJ, Messner SJ, Meschino WS, Piron CA, Narod SA. Surveillance of BRCA1 and BRCA2 mutation carriers with magnetic resonance imaging, ultrasound, mammography, and clinical breast examination. JAMA 2004;292:1317-25.
6. Berg WA, Blume JD, Cormack JB, Mendelson EB,

Lehrer D, Bohm-Velez M, Pisano ED, Jong RA, Evans WP, Morton MJ, Mahoney MC, Larsen LH, Barr RG, Farria DM, Marques HS, Boparai K. Combined screening with ultrasound and mammography vs mammography alone in women at elevated risk of breast cancer. JAMA 2008;299:2151-63.
7. Stavros AT, Thickman D, Rapp CL, Dennis MA, Parker SH, Sisney GA. Solid breast nodules: use of sonography to distinguish between benign and malignant lesions. Radiology 1995;196:123-34.
8. Zonderland HM, Coerkamp EG, Hermans J, van de Vijver MJ, van Voorthuisen AE. Diagnosis of breast cancer: contribution of US as an adjunct to mammography. Radiology 1999;213:413-22.
9. Saslow D, Boetes C, Burke W, Harms S, Leach M, Lehman C, Morris E, Pisano E, Schnall M, Sener S, Smith R, Warner E, Yaffe M, Andrews K, Russell C. American Cancer Society guidelines for breast screening with MRI as an adjunct to mammography. CA Cancer J Clin 2007;57:75-89.
10. Kuhl C, Weigel S, Schrading S, Arand B, Bieling H, Konig R, Tombach B, Leutner C, Rieber-Brambs A, Nordhoff D, Heindel W, Reiser M, Schild HH. Prospective multicenter cohort study to refine management recommendations for women at elevated familial risk of breast cancer: the EVA trial. J Clin Oncol 2010;28:1450-7.
11. Leach MO. MRI for breast cancer screening. Ann Oncol 2006;17 Suppl 10:x325-31.
12. Houssami N, Turner R, Morrow M. Preoperative magnetic resonance imaging in breast cancer: meta-analysis of surgical outcomes. Ann Surg 2013;257:249-55.
13. Berg WA, Gutierrez L, NessAiver MS, Carter WB, Bhargavan M, Lewis RS, Ioffe OB. Diagnostic accuracy of mammography, clinical examination, US, and MR imaging in preoperative assessment of breast cancer. Radiology 2004;233:830-49.
14. Wallace D, Ng J, Keall P, O'Brien R, Poulsen P, Juneja P, Booth J. Determining appropriate imaging parameters for kilovoltage intrafraction monitoring: an experimental phantom study. Phys Med Biol 2015;60:4835-47.
15. Jung J, Song S, Yoon S, Kwak J, Yoon K, Choi W, Jeong S, Choi E, Cho B. Verification of Accuracy of CyberKnife Tumor-tracking Radiation Therapy Using Patient-specific Lung Phantoms. Int J Radiat Oncol Biol Phys 2015;92:745-53.
16. Cowen AR, Brettle DS, Coleman NJ, Parkin GJ. A preliminary investigation of the imaging performance of photostimulable phosphor computed radiography using a

new design of mammographic quality control test object. Br J Radiol 1992;65:528-35.

17. Law J. A new phantom for mammography. Br J Radiol 1991;64:116-20.

18. Huda W, Sajewicz A, Ogden K, Scalzetti E, Dance D. How good is the ACR accreditation phantom for assessing image quality in digital mammography? Acad Radiol 2002;9:764-72.

19. Carton AK, Bakic P, Ullberg C, Derand H, Maidment AD. Development of a physical 3D anthropomorphic breast phantom. Med Phys 2011;38:891-6.

20. White DR. The formulation of tissue substitute materials using basic interaction data. Phys Med Biol 1977;22:889-99.

21. Argo WP, Hintenlang K, Hintenlang DE. A tissue-equivalent phantom series for mammography dosimetry. J Appl Clin Med Phys 2004;5:112-9.

22. Madsen EL, Zagzebski JA, Banjavie RA, Jutila RE. Tissue mimicking materials for ultrasound phantoms. Med Phys 1978;5:391-4.

23. Sun C, Pye SD, Browne JE, Janeczko A, Ellis B, Butler MB, Sboros V, Thomson AJ, Brewin MP, Earnshaw CH, Moran CM. The speed of sound and attenuation of an IEC agar-based tissue-mimicking material for high frequency ultrasound applications. Ultrasound Med Biol 2012;38:1262-70.

24. Cannon LM, Fagan AJ, Browne JE. Novel tissue mimicking materials for high frequency breast ultrasound phantoms. Ultrasound Med Biol 2011;37:122-35.

25. Prokop AF, Vaezy S, Noble ML, Kaczkowski PJ, Martin RW, Crum LA. Polyacrylamide gel as an acoustic coupling medium for focused ultrasound therapy. Ultrasound in Medicine & Biology 2003;29:1351-8.

26. Fujisaki T, Kimura M, Saitoh H, Abe S, Hiraoka T. Production design and evaluation of a novel breast phantom with various breast glandular fractions. Radiat Med 2006;24:647-52.

27. Vieira SL, Pavan TZ, Junior JE, Carneiro AA. Paraffin-gel tissue-mimicking material for ultrasound-guided needle biopsy phantom. Ultrasound Med Biol 2013;39:2477-84.

28. Tuong B, Gardiner I. Development of a novel breast MRI phantom for quality control. AJR Am J Roentgenol 2013;201:W511-5.

29. Freed M, de Zwart JA, Loud JT, El Khouli RH, Myers KJ, Greene MH, Duyn JH, Badano A. An anthropomorphic phantom for quantitative evaluation of breast MRI. Med Phys 2011;38:743-53.

30. Mazzara GP, Briggs RW, Wu Z, Steinbach BG. Use of a modified polysaccharide gel in developing a realistic breast phantom for MRI. Magn Reson Imaging 1996;14:639-48.

31. Liney GP, Tozer DJ, Turnbull LW. A simple and realistic tissue-equivalent breast phantom for MRI. J Magn Reson Imaging 1999;10:968-71.

32. Wengert GJ, Pinker K, Helbich TH, Vogl WD, Spijker SM, Bickel H, Polanec SH, Baltzer PA. Accuracy of fully automated, quantitative, volumetric measurement of the amount of fibroglandular breast tissue using MRI: correlation with anthropomorphic breast phantoms. NMR Biomed 2017;30.

33. Prionas ND, Huang SY, Boone JM. Experimentally determined spectral optimization for dedicated breast computed tomography. Med Phys 2011;38:646-55.

34. Freed M, Badal A, Jennings RJ, de las Heras H, Myers KJ, Badano A. X-ray properties of an anthropomorphic breast phantom for MRI and x-ray imaging. Phys Med Biol 2011;56:3513-33.

35. Madsen EL, Hobson MA, Frank GR, Shi H, Jiang J, Hall TJ, Varghese T, Doyley MM, Weaver JB. Anthropomorphic breast phantoms for testing elastography systems. Ultrasound Med Biol 2006;32:857-74.

36. Ruschin M, Davidson SR, Phounsy W, Yoo TS, Chin L, Pignol JP, Ravi A, McCann C. Technical Note: Multipurpose CT, ultrasound, and MRI breast phantom for use in radiotherapy and minimally invasive interventions. Med Phys 2016;43:2508.

37. Sirtoli VG, Morcelles K, Bertemes-Filho P. Electrical properties of phantoms for mimicking breast tissue. Conf Proc IEEE Eng Med Biol Soc 2017;2017:157-60.

38. Pogue BW, Patterson MS. Review of tissue simulating phantoms for optical spectroscopy, imaging and dosimetry. J Biomed Opt 2006;11:041102.

39. Li W, Belmont B, Greve JM, Manders AB, Downey BC, Zhang X, Xu Z, Guo D, Shih A. Polyvinyl chloride as a multimodal tissue-mimicking material with tuned mechanical and medical imaging properties. Med Phys 2016;43:5577.

40. Liao YL, Chen HB, Zhou LH, Zhen X. Construction of an anthropopathic abdominal phantom for accuracy validation of deformable image registration. Technol Health Care 2016;24 Suppl 2:S717-23.

41. de Carvalho IM, De Matheo LL, Costa Junior JF, Borba Cde M, von Kruger MA, Infantosi AF, Pereira WC. Polyvinyl chloride plastisol breast phantoms for ultrasound imaging. Ultrasonics 2016;70:98-106.

42. Bloch NB, Jain A, Jaffe CC. Data From BREAST-DIAGNOSIS. The Cancer Imaging Archive 2015. Available online: https://wiki.cancerimagingarchive.net/

display/

43. Clark K, Vendt B, Smith K, Freymann J, Kirby J, Koppel P, Moore S, Phillips S, Maffitt D, Pringle M, Tarbox L, Prior F. The Cancer Imaging Archive (TCIA): maintaining and operating a public information repository. J Digit Imaging 2013;26:1045-57.

44. Ju SG, Kim MK, Hong CS, Kim JS, Han Y, Choi DH, Shin D, Lee SB. New technique for developing a proton range compensator with use of a 3-dimensional printer. Int J Radiat Oncol Biol Phys 2014;88:453-8.

45. Müller A, Krishnan KG, Uhl E, Mast G. The application of rapid prototyping techniques in cranial reconstruction and preoperative planning in neurosurgery. J Craniofac Surg 2003;14:899-914.

46. Wagner JD, Baack B, Brown GA, Kelly J. Rapid 3-dimensional prototyping for surgical repair of maxillofacial fractures: a technical note. J Oral Maxillofac Surg 2004;62:898-901.

47. Prionas ND, Lindfors KK, Ray S, Huang SY, Beckett LA, Monsky WL, Boone JM. Contrast-enhanced dedicated breast CT: initial clinical experience. Radiology 2010;256:714-23.

48. Lee MY, Chang CC, Ku YC. New layer-based imaging and rapid prototyping techniques for computer-aided design and manufacture of custom dental restoration. J Med Eng Technol 2008;32:83-90.

49. Dai KR, Yan MN, Zhu ZA, Sun YH. Computer-aided custom-made hemipelvic prosthesis used in extensive pelvic lesions. J Arthroplasty 2007;22:981-6.

50. Hazelaar C, van Eijnatten M, Dahele M, Wolff J, Forouzanfar T, Slotman B, Verbakel W. Using 3D printing techniques to create an anthropomorphic thorax phantom for medical imaging purposes. Med Phys 2018;45:92-100.

51. Rengier F, Mehndiratta A, Von Tenggkobligk H, Zechmann CM, Unterhinninghofen R, Kauczor H, Giesel FL. 3D printing based on imaging data: review of medical applications. Int J Comput Assist Radiol Surg 2010;5:335-41.

52. Liao Y, Wang L, Xu X, Chen H, Chen J, Zhang G, Lei H, Wang R, Zhang S, Gu X, Zhen X, Zhou L. An anthropomorphic abdominal phantom for deformable image registration accuracy validation in adaptive radiation therapy. Med Phys 2017;44:2369-78.

53. Hungr N, Long JA, Beix V, Troccaz J. A realistic deformable prostate phantom for multimodal imaging and needle-insertion procedures. Med Phys 2012;39:2031-41.

54. Rakow-Penner R, Daniel B, Yu H, Sawyer-Glover A, Glover GH. Relaxation times of breast tissue at 1.5 T and 3T measured using IDEAL. Journal of Magnetic Resonance Imaging 2006;23:87-91.

55. Spirou G, Oraevsky A, Vitkin I, Whelan W. Optical and acoustic properties at 1064 nm of polyvinyl chloride-plastisol for use as a tissue phantom in biomedical optoacoustics. Phys Med Biol 2005;50:N141-53.

56. Madsen EL, Frank GR, Krouskop TA, Varghese T, Kallel F, Ophir J. Tissue-mimicking oil-in-gelatin dispersions for use in heterogeneous elastography phantoms. Ultrason Imaging 2003;25:17-38.

57. Madsen EL, Zagzebski JA, Frank GR, Greenleaf JF, Carson PL. Anthropomorphic breast phantoms for assessing ultrasonic imaging system performance and for training ultrasonographers: part I. J Clin Ultrasound 1982;10:67-75.

58. Madsen EL, Zagzebski JA, Frank GR, Greenleaf JF, Carson PL. Anthropomorphic breast phantoms for assessing ultrasonic imaging system performance and for training ultrasonographers: part II. J Clin Ultrasound 1982;10:91-100.

59. Fitzgerald M, White D, White E, Young J. Mammographic practice and dosimetry in Britain. Br J Radiol 1981;54:212-20.

60. Kimme-Smith C, Bassett L, Gold R. A review of mammography test objects for the calibration of resolution, contrast, and exposure. Med Phys 1989;16:758-65.

61. Thompson SR, Faulkner K. A phantom for the measurement of contrast detail performance in film-screen mammography. Br J Radiol 1991;64:1049-55.

62. Obenauer S, Hermann KP, Grabbe E. Dose reduction in full-field digital mammography: an anthropomorphic breast phantom study. Br J Radiol 2003;76:478-82.

63. Suryanarayanan S, Karellas A, Vedantham S, Sechopoulos I, D'Orsi CJ. Detection of simulated microcalcifications in a phantom with digital mammography: effect of pixel size. Radiology 2007;244:130-7.